Available online at www.sciencedirect.com
ScienceDirect
Journal of the European Ceramic Society 27 (2007) 2369–2376
www.elsevier.com/locate/jeurceramsoc

Rutile-type dense ceramics fabricated by pressureless sintering of $Ti_{1-x}Ru_xO_2$ powders prepared by sol–gel

M.T. Colomer*, M.J. Velasco

Instituto de Cerámica y Vidrio, CSIC, C/Kelsen no. 5, 28049 Madrid, Spain

Received 29 June 2006; received in revised form 29 August 2006; accepted 10 September 2006
Available online 2 November 2006

Abstract

Materials in the TiO_2–RuO_2 system, in different shapes, as thin films, coatings, fine powders, xerogels and aerogels are of great interest for many applications, such as energy storage and production systems, solar cells, chemical sensors, electronics, gas separation processes, and industrial electrochemistry. However, a serious drawback in the processing of materials based on RuO_2 is the well-established chemical reactivity above ~700 °C where RuO_2 becomes volatile and oxidizes to RuO_3/RuO_4 gases (in air) or reduces to Ru metal (in a vacuum). For this reason, it is not obvious to attain dense materials in the systems containing Ru. In this study, a novel method has been used to obtain rutile-type $Ti_{1-x}Ru_xO_2$ ($x = 0.05$, 0.08 and 0.10) as dense ceramics without the use of the hot-pressing for the sintering step. The relative densities of the materials prepared were higher than 99.0 ρ_{th} %). This method combines the sol–gel synthesis, a pressureless fast-firing method (heating and cooling rate of 20 °C min^{-1}) at 1350 °C for 10 min and the use of a buffer during the sintering that provides a $RuO_3 + RuO_4$ rich atmosphere.
© 2006 Elsevier Ltd. All rights reserved.

Keywords: Sol–gel processes; Powders-chemical preparation; Sintering; TiO_2

1. Introduction

Materials in the TiO_2–RuO_2 system, in different shapes, as thin films, coatings, fine powders, xerogels and aerogels are of great interest for many applications, such as energy storage and production systems, solar cells, chemical sensors, electronics, gas separation processes, and industrial electrochemistry.[1] It has motivated the further development of processing technologies for their preparation.[2–10] In this regard, the sol–gel process may serve as a good approach to prepare oxide powders or films of this system and several studies have been found in the literature about it.[2–9] The advantage of using this technique is that one could find electrode structures which possess in principle a uniform and homogeneous distribution of electrocatalytically active ruthenium contacts throughout the electrode microstructure, which is not possible to obtain by the conventional decomposition methods. However, a serious drawback in the processing of materials based on RuO_2 is the well-established chemical reactivity above ~700 °C where RuO_2 becomes volatile and oxidizes to RuO_3/RuO_4 gases (in air) or reduces to Ru metal (in a vacuum).[11] The advantage of adding a second oxidic phase, such as ZrO_2, TiO_2, etc., is not only to reduce costs but also to provide a stabilization of the RuO_2 phase against oxidation or reduction processes.

The efficiency of electron conduction in an electrode depends largely on the generated microstructure.[12] The parameters that constitute the microstructure are determined by the synthesis approach and the thermal treatment given to the electrode. All materials based on TiO_2–RuO_2 and pressureless sintered at high temperature reported to date were porous ceramics or porous layered electrodes[13–21] due to the partial RuO_2 volatilization process mentioned above. It places restrictions on their possible applications. Raming et al.[22] prepared dual-phase nanocomposite powders of tetragonal-ZrO_2 doped with 3 mol% Y_2O_3 and RuO_2 and densified them into compacts by hot-pressing. However, the sinterforging or hot-pressing method is an expensive sintering method and is not always available in the laboratory. An attempt to attain dense materials using a $RuO_3 + RuO_4$ rich atmosphere and a fast-firing method was tested by Colomer and Jurado.[23] These authors obtained ceramic materials with compositions $[(ZrO_2)_{0.92}(Y_2O_3)_{0.08}]_{1-x}(RuO_2)_x$, where $x = 0$, 0.05, 0.08 and 0.10 mol, prepared by the conventional solid-state reaction. Despite the use of a $RuO_3 + RuO_4$ rich atmosphere and

* Corresponding author. Tel.: +34 91 735 58 58; fax: +34 91 735 58 43.
E-mail address: tcolomer@icv.csic.es (M.T. Colomer).

0955-2219/$ – see front matter © 2006 Elsevier Ltd. All rights reserved.
doi:10.1016/j.jeurceramsoc.2006.09.006

a fast-firing method (heating and cooling rate of 20 °C min^{-1}) the samples obtained after sintering at temperatures between 900 and 1400 °C exhibited high porosity and contained no Ru or less than that of the nominal composition due to a complete or partial volatilization of RuO_2, respectively. For this reason, the sol–gel method is employed in this study. This synthesis method together with an adequate thermal treatment and atmosphere can provide the attainment of a Ru–O–Ti tridimensional network that allows the preparation of dense $Ti_{1-x}Ru_xO_2$ solid solutions. Furthermore, the understanding of both the hydrolysis and the polycondensation processes of the sol–gel synthesis, could improve both the synthesis method and consequently the materials obtained and their electrocatalytical properties.

In the present work, TiO_2–RuO_2 ceramics were attained as dense materials by pressureless sintering for the first time, as our best knowledge, combining the sol–gel synthesis, a fast-firing method and the use of a buffer during the sintering process.

2. Experimental

Gels with nominal compositions $Ti_{1-x}Ru_xO_2$, where $x = 0.05$, 0.08, and 0.10, were prepared by a polymeric sol–gel method. RuO_2 was also prepared by the sol–gel route, from Ru(III) acetyl-acetonate (acac), in order to attain powder with a high specific surface area for the generation of a $RuO_3 + RuO_4$ atmosphere during the sintering of the pellets. Gels were prepared from Merck analytical grade Ru(III) acetyl-acetonate (acac) and 98% Ti(IV)-iso-propoxide purchased from Janssen. In this method, absolute ethanol (Panreac) was used as medium and water was added as 3 M HNO_3. The molar ratios employed were Ti(IV)-iso-propoxide:H_2O = 1:1.5 and Ti(IV)-iso-propoxide:H^+ = 1:0.09.

In the first stage, the Ru(III) acac was dissolved in absolute ethanol and the solution was refluxed and stirred at 70 °C for 72 h. Ti(IV)-iso-propoxide was also dissolved in absolute ethanol and the solution was refluxed and stirred at 70 °C for 24 h. After that, the latter solution was added to the Ru(III) acac solution and the mixture was refluxed with continuous stirring at 70 °C for 24 h. Ti(IV)-iso-propoxide in ethanol can be stabilized against fast hydrolysis by the presence of acetylacetonate present in the Ru(III) acac solution. Finally, 3 M HNO_3 was added as necessary to reach a Ti(IV)-iso-propoxide:H_2O ratio of 1:1.5. The H^+ acts as a catalyst in the hydrolysis process. The resulting solution was refluxed at 70 °C with stirring for 192 h.

In order to limit solvent evaporation, gels were dried very slowly by covering them with a plastic film. Holes were made in the film with a needle to control the speed of evaporation.[24] The gels were thermally treated in air after milling at 200 and 300 °C for 12 h and at 400 °C for 36 h to assure the complete transformation of anatase to rutile phase and at 500 °C for 1 h to eliminate the organic matter. Higher temperatures or longer times were not used in order to avoid the segregation of the RuO_2 that lead to phase separation.[25] The resulting powder was sieved at 35 μm and pressed (axial and isostatically, 200 MPa). BET specific surface area of the powders was determined using a Monosorb Analyzer MS-13 QuantaChrome. Fourier Transform Infrared Spectroscopy (FTIR) spectra were obtained between 4000 and 400 cm^{-1} for the solutions, the gels and the calcined powders. For the liquid samples KRS-5 crystals were used. A drop of liquid was put on one crystal and then covered by another crystal. For solid samples, ~0.8 mg of a sample was mixed with 300 mg of KBr. The IR spectra were obtained with a Perkin-Elmer 1330 spectrophotometer with a 3600 data station, using the standard program CDS-13 for data handling. Differential thermal and thermogravimetric analyses (DTA–TGA) were carried out by using a Netzsch STA-409 thermoanalyzer under dry air, employing a platinum crucible and a heating and a cooling rate of 20 °C min^{-1} up to 1350 °C, in order to observe the processes involved. As a reference substance finely powdered alumina was used. Crystallinity was evaluated by XRD (Siemens D-5000 Diffractometer) using Cu Kα radiation and a Ni filter. The experimental diffraction patterns were collected at room temperature over a range of $20 \leq 2\theta \leq 80$ (step-scanned at 0.025°/20 s). The morphology of the powders and the microstructure of the sintered materials were observed by means of scanning electron microscopy-energy dispersive X-ray spectroscopy (SEM–EDX) (Model DSM 950, Zeiss, Oberchen, Germany). Transmission electron microscopy-energy dispersive X-ray spectroscopy (TEM–EDX) (JEOL JEM-2010) was used for analyzing the calcined powders. The microstructure of the sintered samples was analyzed on polished and thermal etched surfaces.

Pellets were sintered at 1350 °C for 10 min by rapid firing, at a heating and a cooling rate of 20 °C min^{-1}, and a $RuO_3 + RuO_4$ rich atmosphere (Fig. 1), to minimize ruthenium oxide volatilization losses. This atmosphere is created by the partial volatilization of RuO_2 powder with high specific surface area (38.6 m^2 g^{-1}) attained from Ru(III) acac by the sol–gel method. As is mentioned above, when RuO_2 is heated in the presence of oxygen, the following two reversible reactions have been reported to occur[26,27]:

$$RuO_2(s) + \tfrac{1}{2}O_2(g) \leftrightarrow RuO_3(g)$$

$$RuO_2(s) + O_2(g) \leftrightarrow RuO_4(g)$$

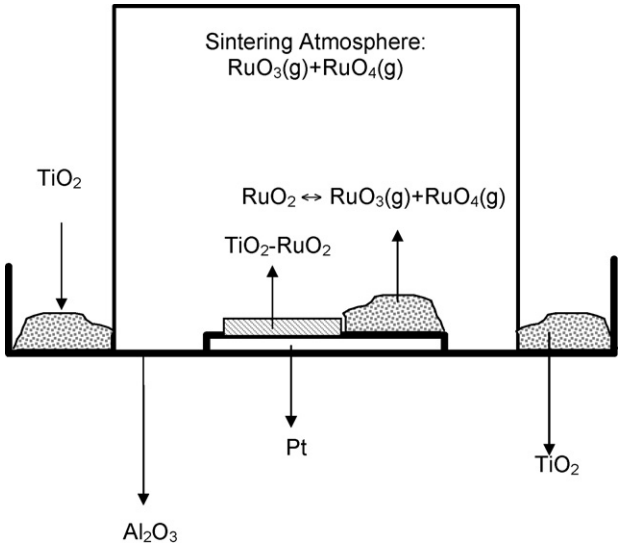

Fig. 1. Schematic representation of the buffer sintering conditions.

The predominant species in the gas phase at temperatures greater than 1000 °C is RuO_3 and at lower temperatures (800 °C) is RuO_4.[26,27] It suggests that RuO_4 and/or RuO_3 may be present on the surface of RuO_2.[28] The furnace employed for sintering was a Rapid High-Temperature Furnace (Bulten-Kanthal AB, S-73401 Hallstahammar, Sweden). Final densities were measured by the Archimedes immersion technique in water, using three pellets attained under nominally identical conditions. Reported values are the average of the three values and errors are the standard deviations. Relative densities were calculated as percentage of the calculated theoretical density, for each composition, from experimental lattice parameters and using 4.25 g cm^{-3} for rutile–TiO_2 (ASTM 21-1276).

In the following, anatase solid solution (Ti,Ru)O_2 will be labeled Ass, and rutile solid solution (Ti,Ru)O_2 will be labeled Rss. Furthermore, the compositions studied in this work will be labeled $100(1-x)$T$100x$R, where $x = 0.05$, 0.08, and 0.10.

3. Results and discussion

3.1. Infrared spectroscopy

3.1.1. Infrared spectroscopy precursors study

At different times, aliquots from the sols were collected to take the IR spectra, in order to follow the hydrolysis and polycondensation reactions. Fig. 2 shows the infrared spectrum of each of the precursors employed. Fig. 2a corresponds to the Ru(III) acetyl-acetonate and Fig. 2b corresponds to the Ti(IV)-iso-propoxide, respectively.

The Ru(III) acetyl-acetonate spectrum (Fig. 2a) shows a band located at 3075 cm^{-1} that corresponds to the stretching vibration of the C–H bond joined to a double bond (=CH–). Bands attributed to the symmetric and non-symmetric stretching mode of the $-CH_3$ bond appear at 2965 and 2920 cm^{-1}, respectively.

The most characteristic bands of the Ru(III) acetyl-acetonate correspond to the carbonyl group located at 1545 and 1515 cm^{-1} (ν_1 and ν_2, respectively). These values are in accord to those of Endo et al.[29] These bands appear as a doublet and at lower frequencies than that of a free C=O bond (1700 cm^{-1}), indicating both a conjugation with a C=C double bond[30] and that the carbonyl group is part of a cyclic structure. The band corresponding to the above mentioned C=C double bond appears at 1590 cm^{-1} (ν_3) as a shoulder overlapped with the carbonyl group bands. Another characteristic band is located at 953 cm^{-1} (ν_4), and is assigned to the Ru–O–C bond.[15]

Other bands present in the IR spectrum of the Ru(III) acac are located at 1365 and 1270 cm^{-1}. The first one is ascribed to the C–H bond deformation in a $-CH_3$ group, which is very intense due to the C–H bond joined to a carbonyl group. The second band is assigned to the deformation of a C–H group joined with a double bond.

The spectrum of the Ti(IV)-iso-propoxide (Fig. 2b) shows three bands at 2970, 2930 and 2867 cm^{-1} corresponding to the stretching mode of the C–H bond in the groups $-CH_3$ and $-CH_2$. The deformation bands due to those groups appear in the spectrum between 1500 and 1300 cm^{-1}.

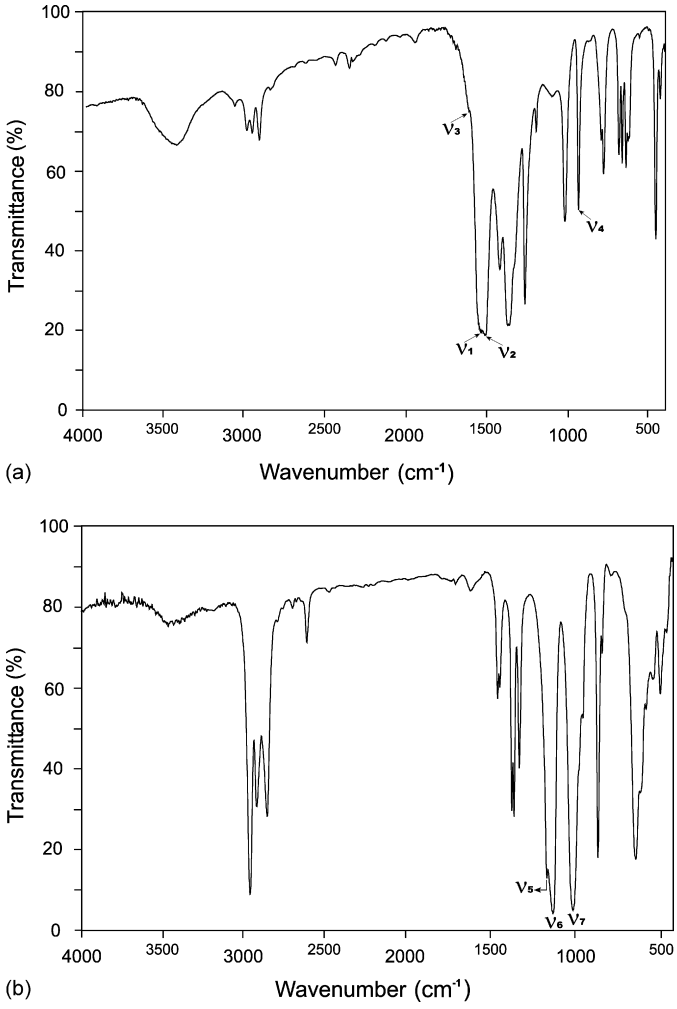

Fig. 2. IR spectrum of each of the precursors employed. (a) Ru(III) acac. The most characteristic bands of the Ru(III) acetyl-acetonate correspond to the carbonyl group located at 1545 and 1515 cm^{-1} (ν_1 and ν_2, respectively). Another characteristic band is located at 953 cm^{-1} (ν_4), and is assigned to the Ru–O–C bond.[15] (b) Ti(IV)-iso-propoxide. The most characteristic bands of the Ti(IV)-iso-propoxide are due to the Ti–O–C stretching bond and are located at 1160, 1125 and 1005 cm^{-1} (ν_5, ν_6 and ν_7, respectively).[30]

The most characteristic bands of the Ti(IV)-iso-propoxide are due to the Ti–O–C stretching bond and are located at 1160, 1125 and 1005 cm^{-1} (ν_5, ν_6 and ν_7, respectively).[30] The bands corresponding to the deformation vibration of the C–H, C–O and Ti–O bonds appear in the 900–400 cm^{-1} region.

According to these results, the hydrolysis reactions of the Ti(IV)-iso-propoxide and Ru(III) acac can be followed by means of (1) the decreasing intensities of the bands at 1160, 1125 and 1005 cm^{-1} (Ti–O–C) (ν_5, ν_6 and ν_7, respectively) due to the rupture of the Ti–O bonds, present in Ti(IV)-iso-propoxide, (2) the shifts of the frequencies of the C=O bond at 1545 and 1515 cm^{-1} (ν_1 and ν_2, respectively) due to the formation of a free diketone from the rupture of the cyclic ring of the Ru(III) acac and (3) the decreasing intensity of the band located at 953 cm^{-1} (Ru–O–C) (ν_4) present in the Ru(III) acac. The polycondensation reactions can be followed by both the appearance and intensity increase of the bands corresponding to the Ru–O–Ru, Ru–O–Ti and Ti–O–Ti bonds.

3.1.2. Infrared spectroscopy mixtures study

In order to better evaluate the IR spectra, and due to the high amount of ethanol required for the Ru(III) acac dissolution, each aliquot of the sols was concentrated to eliminate part of the alcohol (ethanol). For this reason, the isopropanol formed during the polycondensation process is also eliminated and is not observed by IR spectroscopy.

In Fig. 3a–c the IR spectra of the resulting sols at different times are shown.

In Fig. 3a the IR spectrum of the precursors mixture for the sol with $x = 0.10$ at time = 0 is shown, before solvent evaporation. Fig. 3b and c show the IR spectrum of the same sol after 4 and 8 days of reaction and solvent evaporation, respectively.

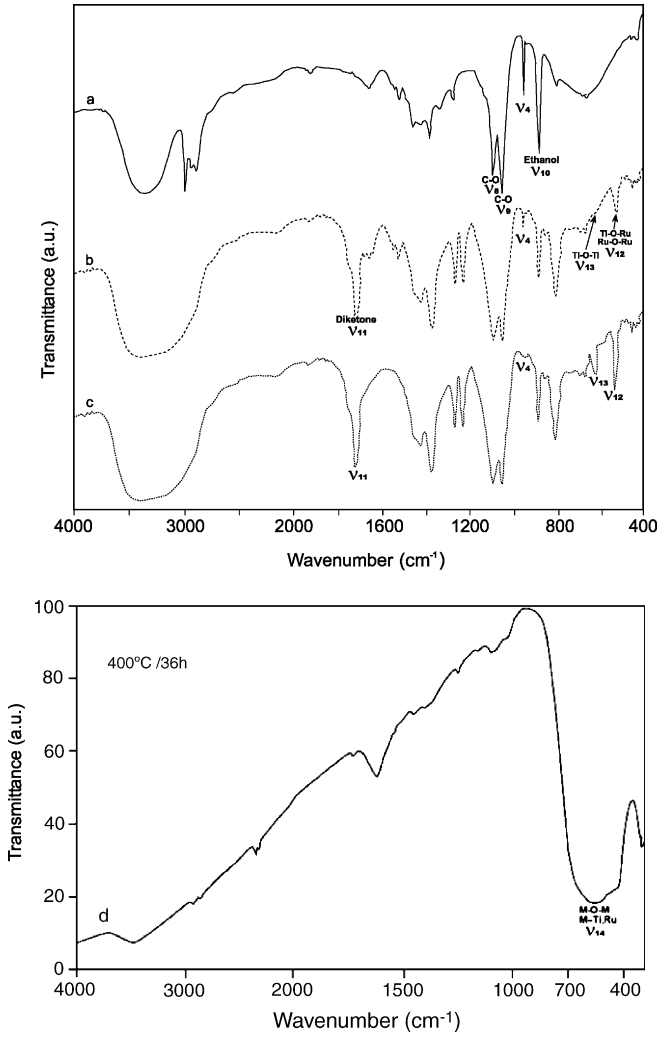

Fig. 3. (a) IR spectrum of the mixture of precursors for the sol 90T10R at time = 0 s. (b) IR spectrum of the same sol after 4 days of reaction with partial solvent evaporation. (c) IR spectrum of the same sol after 8 days of reaction with partial solvent evaporation. The hydrolysis of the Ru(III) acac can be deduced because a decrease in the intensity of the υ_4 band is detected. The intensity increase of the band situated at 1700 cm^{-1} (ν_{11}), and corresponding to the C=O bond of the formed diketone indicates, among other band intensity modifications, that the hydrolysis reaction is very advanced. (d) IR spectrum of the xerogel 90T10R calcined at 400 °C for 36 h. The wide band observed in the frequency range, 800–450 cm^{-1} (ν_{14}), is ascribed to the Ti—O—Ti and Ti—O—Ru bonds formed during the polycondensation reactions.[15,31]

In Fig. 3a, the bands corresponding to the ethanol are mostly observed. The precursor bands are almost negligible. At 3330 cm^{-1}, the stretching vibration corresponding to the O–H bond is detected and at about 3000 cm^{-1} the stretching modes of the $–CH_3$ and $–CH_2$ groups appear. In the spectral region from 1200 to 800 cm^{-1} three typical bands from the ethanol appear: $\upsilon_{8,C–O}$: 1090 and $\upsilon_{9,C–O}$: 1050 cm^{-1} and the skeletal vibration of the molecule at 880 cm^{-1} (ν_{10}).

Fig. 3b shows at 1710 cm^{-1} a sole band that can be ascribed to the stretching vibration of the C=O bond (ν_{11}). This band is shifted to higher frequencies than that in the Ru(IIII) acac due to the rupture of the ring in the molecule. This band is slightly shifted compared with that of a free carbonyl group. This shifting is due to the presence of two different resonant structures, keto and enol structures. Thus, the formation of a diketone from the rupture of the C–O–Ru bond is obtained. Together with this latter band, two bands that correspond to the C=O bond of the Ru(IIII) acac coexist at 1545 and 1515 cm^{-1} (ν_1 and ν_2, respectively). These two bands present a low intensity, indicating that, at those reaction times, part of the Ru(IIII) acac has not been hydrolyzed yet.

The rupture of the C–O–Ru bond can be observed from the band located at 953 cm^{-1} (ν_4 in the mixture, Fig. 3a–c). The hydrolysis of the Ru(III) acac can be deduced because a decrease in the intensity of that band is detected.

The bands corresponding to the Ti–O–C bond of the Ti(IV)-iso-propoxide (bands at 1160, 1125 and 1005 cm^{-1}) appear as a shoulder overlapped with the bands located at 1090 and 1050 cm^{-1} from the ethanol (ν_8 and ν_9, respectively). This could indicate that hydrolysis of the Ti(IV)-iso-propoxide takes place. On the other hand, a band located at 533 cm^{-1} (ν_{12}) could be assigned to the Ti–O–Ru and/or Ru–O–Ru and a shoulder located at ~652 cm^{-1} (ν_{13}) can be attributed to the Ti–O–Ti bond formation[31] during the polycondensation reactions.

In Fig. 3c (8 days of reaction) the disappearance of the bands situated at 1515 (ν_1) and 1545 cm^{-1} (ν_2), corresponding to the C=O bond of the Ru(III) acac, the increase of the one situated at 953 cm^{-1} (ν_4), assigned to the Ru–O–C bond,[15] and the intensity increase of the band situated at 1700 cm^{-1} (ν_{11}), and corresponding to the C=O bond of the formed diketone indicate that the hydrolysis reaction is very advanced.

The Ti–O–C bands that appeared as a shoulder overlapping with the bands of the ethanol at 1090 and 1050 cm^{-1} at the spectrum 3b are not longer visible, indicating the rupture of these bonds.

In Fig. 3c an intensity increase of the bands at 652 cm^{-1} (Ti–O–Ti) and at 533 cm^{-1} (Ru–O–Ru or Ti–O–Ru) is also observed, indicating the extent of the polycondensation reaction.

Fig. 3d shows the infrared spectrum of the xerogel 90T10R calcined at 400 °C/36 h. During the calcination, the bands corresponding to the organic groups disappear. Heat treatment at this temperature causes elimination of the peaks due to OH, CH, C–OH, Ti–O–C and Ru–O–C chemical groups, and the subsequent formation of Ti–O–Ti, Ru–O–Ru and Ru–O–Ti bonds. The wide band observed in the frequency range, 800–450 cm^{-1} (ν_{14}), is ascribed to the Ti–O–Ti and Ti–O–Ru bonds formed during the polycondensation reactions.[15,31,32] The inactive

ruthenium dioxide cannot be positively identified by FTIR[33,34] because is a conductive oxide.

A similar evolution can be observed for the rest of the sols.

4. DTA–TG

Fig. 4a and b show the DTA and TGA curves for the xerogel with $x = 0.05$ (95T5R).

The weak endothermic peak centered at 147 °C could be associated with all the following processes: (a) evaporation of residual absolute ethanol used as solvent in the synthesis, (b) evaporation of water from HNO_3, (c) evaporation of iso-propanol formed during the hydrolysis of Ti(IV)-iso-propoxide, and (d) evaporation of water formed during the polycondensation process. A weight loss of ∼13% detected from room temperature to 210 °C in the TGA curve can be associated with the elimination of those volatile products.

An inflection is observed, at ∼280 °C, in the DTA curve and can be attributed to the loss of the absolute ethanol, iso-propanol, and water trapped in the pores of the gel. This is associated with a weight loss in the range 210–280 °C in the TGA curve. The exothermic peak centered at ∼345 °C is related to the combustion of the various carbonaceous residuals (isopropoxy groups ($–OC_3H_7$), acetylacetonate groups, etc.) that have remained in the matrix of the xerogel. Weight losses are detected in the TGA up to 570 °C and can be attributed to the elimination of these organic groups and to the polycondensation processes is completed. Lastly, an exothermic peak observed at ∼532 °C could be attributed to the rutile formation. This peak is detected at decreasing temperature when the ruthenium content increases (from 560 °C for $x = 0$[25] to 420 °C for $x = 0.10$). All the DTA and TGA curves exhibit similar characteristics for the different studied compositions.

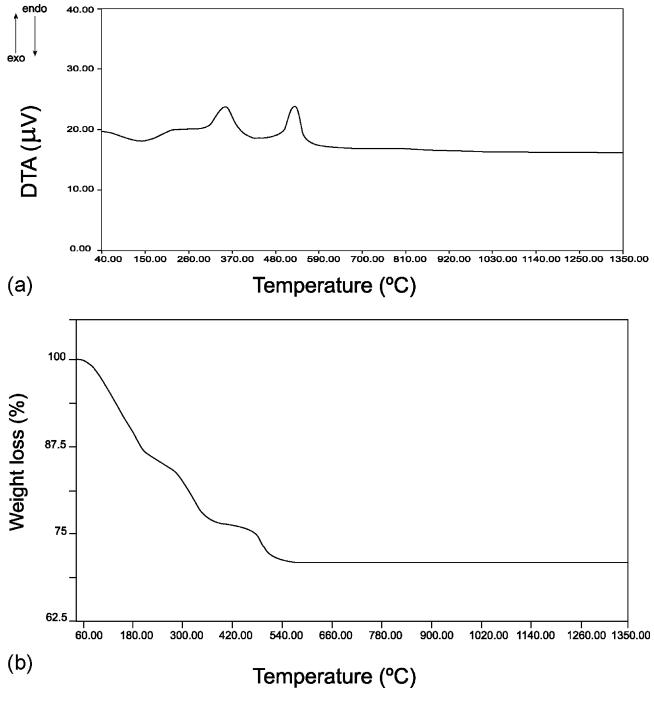

Fig. 4. (a and b) DTA–TGA curves of a 95T5R xerogel.

For all the compositions a rutile solid solution, (Rss), was detected by means of XRD in the residual ash.

A discrepancy in the temperature events during the calcination treatments and during the TG measurements occurs and is due to the fact that TG analysis is a dynamic process. Furthermore, there must be taken into account that the DTA and TGA curves have been collected under dry air, a different atmosphere that the used for the sintering processes.

5. XRD

The XRD patterns of all the dried gels indicated that an amorphous structure was formed at the reaction temperature (70 °C). Table 1 shows the crystalline phases detected in the studied samples calcined at each temperature, 200 and 300 °C for 12 h, and at 400 °C for 36 h. The diffraction peaks could be assigned to the anatase (Ass) and rutile (Rss) structures with d-spacings shifted with respect to the anatase and rutile–TiO_2 phases, respectively. At temperatures, as low as 200 °C, mixtures of both anatase Ass and rutile Rss solid solutions were attained. Mixtures of Ass and Rss solid solutions are also present for all the compositions at 300 °C for 12 h. At 400 °C for 36 h only the Rss solid solution is present. The evolution observed in the intensity of the diffraction peaks is also indicated in Table 1. The solid solution limit of RuO_2 into Rss lattice, is located at least at $x = 0.1$ for samples sintered at 1350 °C. Thus, free RuO_2 has not been detected for the experimental conditions employed in any studied composition.

Controversial data about the solid solution limit of ruthenium oxide into the rutile–TiO_2 lattice can be found in the literature although preferentially referred to films. Levedeb et al.[35] observed for samples prepared by the conventional solid state reaction a narrow region (8–9 mol%, pellets prepared at 1300 °C in air) of solubility of TiO_2 in RuO_2; in the remaining region solid solutions of TiO_2 in RuO_2 coexist with rutile TiO_2. However, our results are not comparable with those because the sintering carried out by Levedeb et al. was in air. According to Málek et al.[9] the $(TiO_2)_x(RuO_2)_{1-x}$ powders crystallized up to 600 °C for $0 \leq x \leq 0.7$ were single phase of rutile-type solid solutions. In the latter case, a dry nitrogen flow for the calcination was used.[9] Again our results are not comparable with those by Málek et al. because of the use of a different atmosphere during the thermal treatment, which implies a different sintering process and thus different materials. Gerrard and Steele[10] reported the presence of separate RuO_2- and TiO_2-rich phases at 800 °C, for films prepared by the conventional thermal decomposition method, indicating that only a very limited solid solubility (less than 1.5 mol% RuO_2) was observed. Guglielmi et al.[2] reported that for 30 mol% RuO_2 films prepared by sol–gel synthesis and calcined at 400 °C, a rutile solid solution is formed and observed by XRD as a unique phase. Kameyama et al.[3] obtained rutile compositions with high RuO_2 content (80 at.%) at 450 °C for 3 h also by the sol–gel method but no dissolution of RuO_2 into TiO_2 was attained for compositions with less than 20 at.% of RuO_2. Hrovat et al.[13] used wavelength dispersive X-ray quantitative

Table 1
Evolution of the crystalline phases for the materials prepared as a function of the temperature

Calcination T (°C), time and atmosphere	Composition		
	95T5R	92T8R	90T10R
200 °C, 12 h in air	↑Ass + ↓Rss	↑Ass + ↓Rss	↑Ass + ↓Rss
300 °C, 12 h in air	↑Ass + ↓Rss	↑Ass + ↓Rss	↑Ass + ↓ Rss
400 °C, 36 h in air	Rss	Rss	Rss
1350 °C, 10 min using buffer	Rss	Rss	Rss

Anatase solid solution $(Ti,Ru)O_2$ is labeled Ass, and the rutile solid solution phase $(Ru,Ti)O_2$ is labeled Rss. The arrow (↑) indicates the phase with the highest intensity peaks and the arrow (↓) indicates the phase with the weakest intensity diffraction peaks, respectively.

microanalysis (WDS) for the investigation of phase equilibria and the extent of solid solubility in the RuO_2–TiO_2 system. The conventional ceramic method was used for the synthesis and the pellets were buried in RuO_2 powder to suppress the evaporation of volatile RuO_3 and RuO_4. The solid solubility at 1350 °C was determined to be 0.135 mol RuO_2 in TiO_2. Our data agree with that given by Hrovat et al.[13] as can be seen in Table 1.

6. SEM–EDX and TEM–EDX

Scarlet colored and translucent gels were obtained for all the compositions. Fig. 5 shows a SEM micrograph of a piece of a dry gel. EDX analysis indicated the presence of Ti and Ru elements in stoichiometric proportions and homogeneously distributed that implies the attainment of a Ru–O–Ti tridimensional network. The sol–gel method allowed us to achieve gels formed by a tridimensional network in which both Ti and Ru ions are involved at 70 °C. After an adequate thermal treatment together with a $RuO_3 + RuO_4$ rich atmosphere the gels give rise to $Ti_{1-x}Ru_xO_2$ solid solutions, where $x = 0.05$, 0.08 and 0.10, up to temperatures as high as 1350 °C.

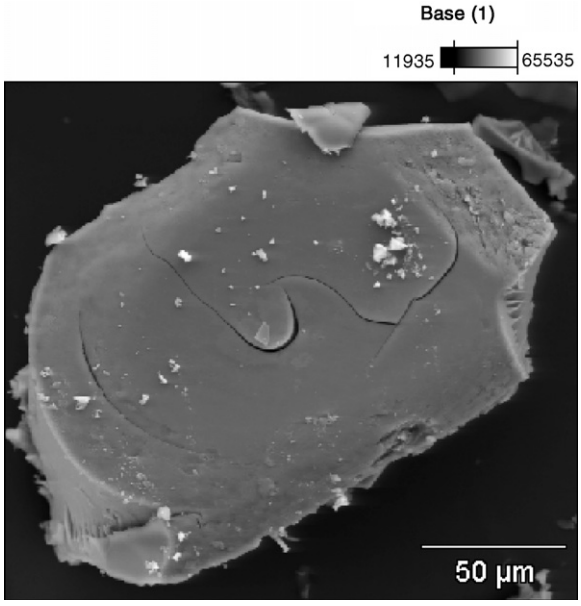

Fig. 5. SEM micrograph of a piece of the xerogel 90T10R.

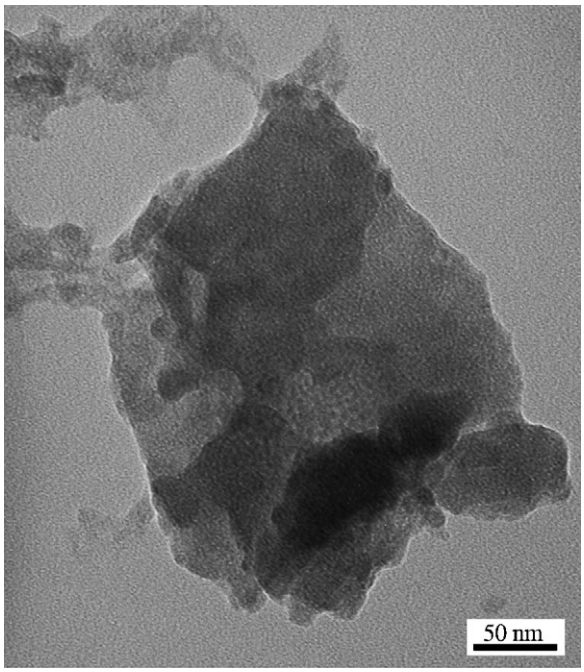

Fig. 6. TEM picture of a 90T10R xerogel after milling.

When the powders, attained after milling the xerogels, are observed by TEM, agglomerates of very fine crystals could be clearly perceived (Fig. 6).

SEM micrographs of polished and thermal etched surfaces of the sintered 90T10R sample are shown in Fig. 7a and b. The EDX semiquantitative analysis indicated the presence of Ti and Ru elements in stoichiometric proportions and confirms the solid solubility of the RuO_2 into the rutile lattice.

Table 2 shows the theoretical, the final and the relative densities of the studied samples. Fully densified bodies were obtained for all cases, i.e., the relative densities were higher than 99.0 ρ_{th} %.

Table 2
Theoretical, final and relative densities of the samples

Material	ρ_{th} (g cm^{-3})	$\rho_{experimental}$ (g cm^{-3})	ρ_{th} (%)
100T	4.25	–	–
95T5R	4.39 ± 0.01	4.36 ± 0.01	99.3 ± 0.1
92T8R	4.55 ± 0.01	4.52 ± 0.01	99.3 ± 0.1
90T10R	4.65 ± 0.01	4.61 ± 0.01	99.1 ± 0.1

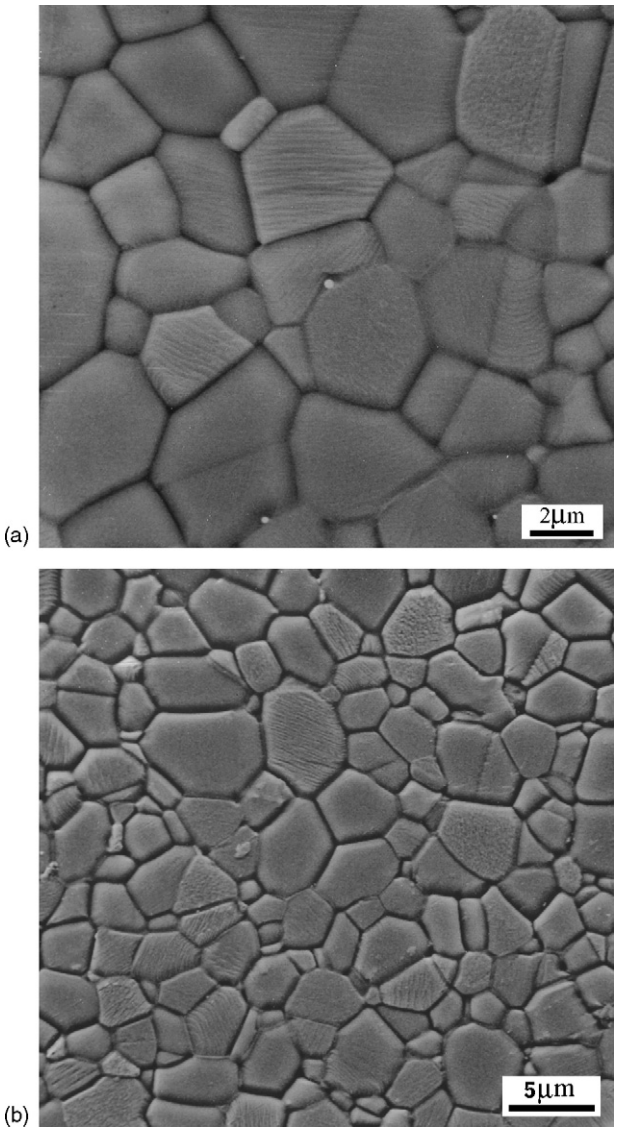

Fig. 7. (a and b) SEM of the 90T10R material after sintering and thermal etching.

7. Conclusion

A novel method has been used to obtain rutile-type, $Ti_{1-x}Ru_xO_2$, single solid solutions as dense ceramics (the relative densities were higher than 99.0 ρ_{th} %). This method combines the sol–gel synthesis, a pressureless fast-firing method (heating and cooling rate of 20 °C min^{-1}) at 1350 °C for 10 min and, the use of a buffer during the sintering that provides a $RuO_3 + RuO_4$ rich atmosphere and prevent the volatilization of RuO_2 from the samples.

Acknowledgments

We gratefully acknowledge to Prof. J.R. Jurado his useful suggestions.

This work is in the frame of the EC Projects JOE3-CT97-0049 and ENK5-CT-2001-00572.

References

1. Pârvulescu, V., Pârvulescu, V. I., Popescu, G., Julbe, A., Guizard, C. and Cot, L., Gas–solid oxidations with RuO_2–TiO_2 and RuO_2–SiO_2 membranes. *Catal. Today*, 1995, **25**, 385–389.
2. Guglielmi, M., Colombo, P., Rigato, V., Battaglin, G., Boscolo-Boscoletto, A. and DeBattisti, A., Compositional and microstructural characterization of RuO_2–TiO_2 catalysts synthesized by the sol–gel method. *J. Electrochem. Soc.*, 1992, **139**, 1655–1661.
3. Kameyama, K., Tsukada, K., Yahikozawa, K. and Takasu, Y., Preparation of ultrafine RuO_2–TiO_2 binary oxide particles by a sol–gel process. *J. Electrochem. Soc.*, 1993, **140**, 1034–1037.
4. Mink, J., Kristof, A., De Battisti, A., Daolio, S. and Nemeth, C. S., Investigation on the formation of RuO_2-based mixed-oxide coatings by spectroscopic methods. *Surf. Sci.*, 1995, **335**, 252–257.
5. Swider, K. E., Merzbacher, C. I., Hagans, P. L. and Rolison, D. R., Synthesis of ruthenium dioxide titanium dioxide aerogels: redistribution of electrical properties on the nanoscale. *Chem. Mater.*, 1997, **9**, 1248–1255.
6. Panic, V. V., Dekanski, A., Milonjic, S. K., Atanasoski, R. T. and Nikolic, B. Z., RuO_2–TiO_2 coated titanium anodes obtained by the sol–gel procedure and their electrochemical behaviour in the chlorine evolution reaction. *Colloids Surf. A Physicochem. Eng. Aspects*, 1999, **157**, 269–274.
7. Zhitomirsky, I., Electrolytic TiO_2–RuO_2 deposits. *J. Mater. Sci.*, 1999, **34**, 2441–2447.
8. Panic, V. V., Dekanski, A., Wang, G., Fedoroff, M., Milonjic, S. and Nikolic, B., Morphology of RuO_2–TiO_2 coatings and TEM characterization of oxide sols used for their preparation. *J. Colloid Interf. Sci.*, 2003, **263**, 68–73.
9. Málek, J., Watanabe, A. and Mitsuhashi, T., Sol–gel preparation of rutile type solid solution in TiO_2–RuO_2 system. *J. Therm. Anal. Calorim.*, 2000, **60**, 699–705.
10. Gerrard, W. A. and Steele, B. C. H., Microstructural investigations on mixed RuO_2–TiO_2 coatings. *J. Appl. Electrochem.*, 1978, **8**, 417–425.
11. Tagirov, V. K., Chizhikov, D. M., Kazenas, E. K. and Shubocchkin, L. K., Thermal dissociation of ruthenium dioxide and rhodium sesquioxide. *J. Inorg. Chem.*, 1977, **20**, 1133–1135.
12. Long, Y. C., Zhang, Z. D., Dwight, K. and Wold, A., Preparation and characterization of ZrO_2 stabilized with Ru(IV) and La(III). *Mater. Res. Bull.*, 1988, **23**, 631–636.
13. Hrovat, M., Holc, J., Samardizja, Z. and Drazic, G., The extent of solid solubility in the RuO_2–TiO_2 system. *J. Mater. Res.*, 1996, **11**, 727–732.
14. Djurado, E., Roux, C. and Hammou, A., Synthesis and structural characterization of a new system: ZrO_2–Y_2O_3–RuO_2. *J. Eur. Ceram. Soc.*, 1996, **16**, 767–771.
15. Colomer, M. T. and Jurado, J. R., Preparation and characterization of gels of the ZrO_2–Y_2O_3–RuO_2 system. *J. Non-Cryst. Solids*, 1997, **217**, 48–54.
16. Colomer, M. T. and Jurado, J. R., Structural, microstructural, and electrical transport properties of TiO_2–RuO_2 ceramic materials obtained by polymeric sol–gel route. *Chem. Mater.*, 2000, **12**, 923–930.
17. Ryan, J. V., Berry, A. D., Anderson, M. L., Long, J. W., Stroud, R. M., Cepak, V. M. *et al.*, Electronic connection to the interior of a mesoporous insulator with nanowires of crystalline RuO_2. *Nature*, 2000, **406**, 169–172.
18. Camara, O. R. and Trassatti, S., Surface electrochemical properties of Ti/($RuO_2 + ZrO_2$) electrodes. *Electrochim. Acta*, 1996, **41**, 419–427.
19. Burke, L. D. and McCarthy, M., Oxygen gas evolution at, and deterioration of, RuO_2/ZrO_2-coated titanium anodes at elevated-temperature in strong base. *Electrochim. Acta*, 1984, **29**, 211–216.
20. Hrovat, M., Holc, J. and Kolar, D., Thick film ruthenium oxide/yttria-stabilized zirconia-based cathode material for solid oxide fuel cells. *Solid State Ionics*, 1994, **68**, 93–98.
21. Hrovat, M., Bernik, S. and Holc, J., Subsolidus phase equilibria in the RuO_2–SrO–ZrO_2 system. *J. Mater. Sci. Lett.*, 1999, **18**, 1019–1020.
22. Raming, T. P., van Zyl, W. E. and Verweij, H., Influence of temperature and pressure on the densification, microstructure, and electrical properties of the dual-phase system Y_2O_3-doped ZrO_2 and RuO_2. *Chem. Mater.*, 2001, **13**, 284–289.
23. Colomer, M. T. and Jurado, J. R., Preparation and characterization of ruthenia-doped yttria-stabilized zirconia ceramics. *J. Solid State Chem.*, 1998, **141**, 282–289.

24. Zarzycki, J., Prassas, M. and Phalippou, J., Synthesis of glasses from gels—the problem of monolith gels. *J. Mater. Sci.*, 1982, **17**, 3371–3379.
25. Colomer, M. T., Velasco, M. J. and Jurado, J. R., Synthesis and thermal evolution of TiO_2–RuO_2 xerogels. *J. Sol–Gel Sci. Technol.*, 2006, **39**, 211–222.
26. Kim, K. S. and Winograd, N. J., X-ray photoelectron spectroscopic studies of ruthenium–oxygen surfaces. *J. Catal.*, 1974, **35**, 66–72.
27. Bell, W. E. and Tagami, M., High-temperature chemistry of ruthenium-oxygen system. *J. Phys. Chem.*, 1963, **67**, 2432.
28. Ji, L., Lin, J. and Zeng, H. C., Thermal processes of volatile RuO_2 in nanocrystalline Al_2O_3 matrixes involving gamma → alpha phase. *Chem. Mater.*, 2001, **13**, 2403–2412.
29. Endo, A., Kajitani, M., Mukaida, M., Shimizu, K. and Sato, G. P., A new synthetic method for ruthenium complexes of β-diketones form 'ruthenium blue solution' and their properties. *Inorg. Chim. Acta*, 1988, **150**, 25–34.
30. Pretch, E., Clerc, T., Seibl, J. and Simon, W., ed., *Tablas para la Elucidación Estructural de Compuestos Orgánicos por Métodos Espectroscópicos, Vol. I*. Alhambra, Madrid, Spain, 1988, p. 135.
31. Doeuff, S., Henry, M., Sanchez, C. and Livage, J., Hydrolysis of titanium alkoxides-modification of the molecular precursor by acetic acid. *J. Non-Cryst. Solids*, 1987, **89**, 206–216.
32. Beghi, M., Chiurlo, P., Costa, L., Palladino, M. and Pirini, M. F., Structural investigation of the silica titania gel glass-transition. *J. Non-Cryst. Solids*, 1992, **145**, 175–179.
33. Bewick, A., Gutiérrez, C. and Larramona, G., In-situ infrared spectroscopic study of the anodic oxide film on iron in alkaline-solution. *J. Electroanal. Chem.*, 1991, **318**, 207–221.
34. Chan, H. Y. H., Takoudis, C. G. and Weaver, M. J., High-pressure oxidation of ruthenium as probed by surface-enhanced Raman and X-ray photoelectron. *J. Catal.*, 1997, **172**, 336–345.
35. Levedeb, V. M., Roginskaya, Y. E., Klimasenko, N. L., Bystrov, V. I. and Venevtsev, Y. N., Effect of preparation methods on phase composition of samples of RuO_2–TiO_2 system. *Zh. Neorg. Khim.*, 1976, **21**, 2511–2515.